Multichannel RRKM Study on the Mechanism and Kinetics of the $CH_3Cl + OH$ Reaction

MARYAM DEHESTANI, FAHIMEH SHOJAIE

Department of Chemistry, Shahid Bahonar University of Kerman, Kerman, Iran

Received 12 February 2011; accepted 28 March 2011
Published online 20 May 2011 in Wiley Online Library (wileyonlinelibrary.com).
DOI 10.1002/qua.23132

ABSTRACT: The kinetics and mechanism of the reaction of OH with CH_3Cl have been theoretically studied. The potential energy surface for each possible pathway has been investigated by the G2MP2 method. The rate constants for channels leading to several products have been calculated by multichannel-Rice-Ramsperger-Kassel-Marcus (RRKM) theory over a temperature range 200–2000 K. The results show the major channel is hydrogen abstraction mechanism. ©2011 Wiley Periodicals, Inc. Int J Quantum Chem 112: 1307–1315, 2012

Key words: multichannel-RRKM theory; G2MP2 method; ab initio calculations; methyl chloride

1. Introduction

Chlorinated alkanes are the potential sources of chlorine in the stratosphere, where they can catalytically destroy ozone [1, 2]. Methyl chloride, the most abundant halocarbon in the atmosphere, has received much attention as a natural source of chlorine atoms in the stratosphere [3, 4]. Hydroxyl radical breaks down and removes many of the gases that pollute the air, including methyl chloride. The reactions of CH_3Cl with various radicals, like OH and H, have been studied [5, 6]. A few ab initio studies of the reactivity of OH toward some chlorosubstituted methanes were performed at various levels of theory [5, 7, 8]. There are two possible pathways for the reaction of CH_3Cl with OH:

$$CH_3Cl + OH \rightarrow CH_2Cl + H_2O \quad (1)$$

$$CH_3Cl + OH \rightarrow CH_3 + HOCl \quad (2)$$

Recently, only the first channel of this reaction has been theoretically investigated by Tzima et al. [9]. But no calculations have been performed for the second reaction path up to now. To understand the title reaction in details, several problems need to be clarified. (1) What are the mechanisms involved, and what are the products? (2) What is the dependence of the rate constants and branching ratio on the temperature? In this article, detailed ab initio calculations are used to study

Correspondence to: M. Dehestani; e-mail: dehestani@mail.uk.ac.ir

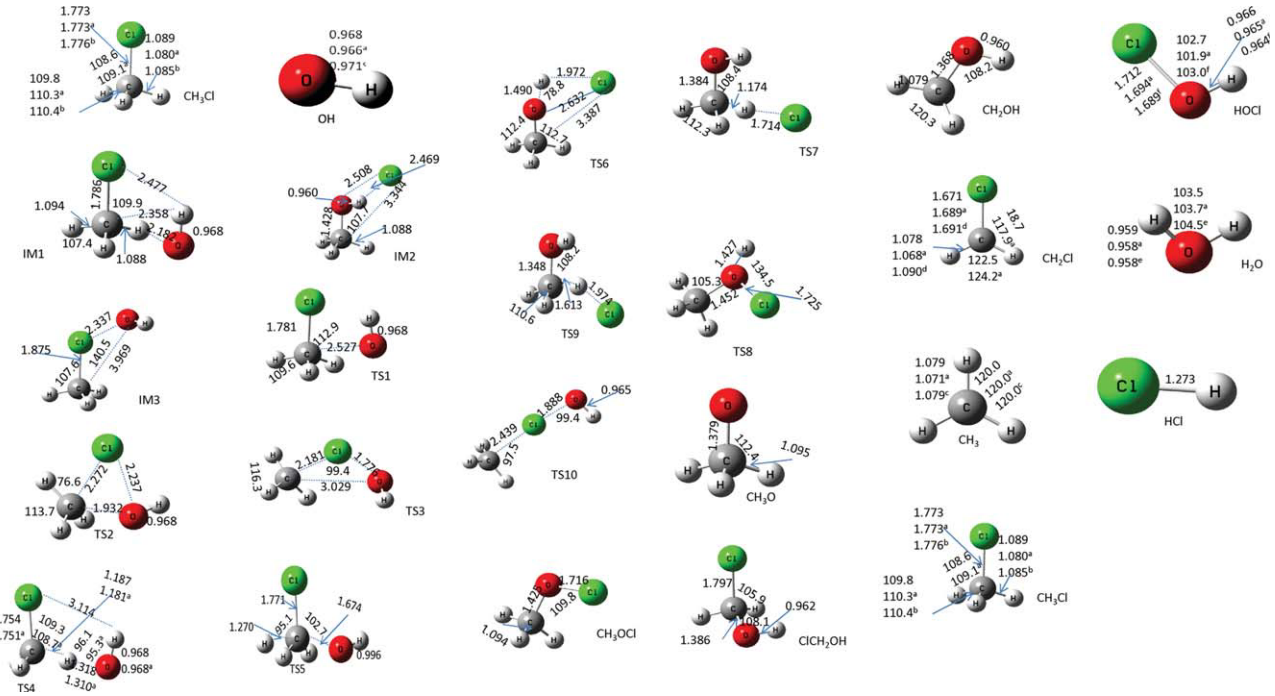

FIGURE 1. Optimized geometries of all the reactants, IMs, TS, and products for the $CH_3Cl + OH$ reaction at the MP2/6-311+G (d, p). Bond lengths are in angstroms and angles are in degrees. [a]Ref. [9], [b]Ref. [15], [c]Ref. [16], [d]Ref. [17], [e]Ref. [18], and [f]Ref. [19]. [Color figure can be viewed in the online issue, which is available at wileyonlinelibrary.com.]

the mechanisms of the title reaction, and the RRKM calculation is implemented to check the kinetics of the multichannel reaction.

2. Computational Methods

Theoretical calculations were carried out for the title reaction using the Gaussian 03 program [10]. The geometries of reactants (R), transition states (TSs), intermediates (IMs), and products (P) were optimized using the MP2/6-311+G (d, p) level of theory. For determining the nature of all species and the zero-point energy (ZPE) corrections, harmonic vibrational frequencies were calculated at the same level. The number 0 or 1 of imaginary frequencies individuates a local minimum or a TS. Subsequently, the intrinsic reaction coordinate (IRC) [11–13] calculations were performed at the same level to verify that the TSs connect the designated reactants and products. To obtain more reliable energies of all the stationary points on the potential energy surface (PES), the G2MP2 method [14] was used to calculate the single point energy at the MP2/6-311+G (d, p) optimized geometries. RRKM calculations have been carried out to obtain the total and individual rate constants and the branching ratio for the various product channels.

3. Results and Discussion

The calculated geometries of all reactants, products, IMs and TSs involved in the reaction of CH_3Cl with OH in the present work are shown in Figure 1 along with experimental geometries [15–19] and theoretical ones of Tzima et al. [9]. The PES of the title reaction at the G2MP2 method is depicted in Figure 2. Table I exhibits the ZPE corrections and relative energies (relative to the reactants of $CH_3Cl + OH$) at the levels of the G2 and the G2MP2. To obtain more reliable energies for rate constant calculation, we have used the G2MP2 method. This table also includes the calculated reaction enthalpy values at 298 K in this study along with the results of PMP4(SDIQ) calculations with 6-311G(3df, 2p) and 6-311++G(3df, 2pd) [5], PMP2(Full) calculations with cc-pVTZ basis set [9] and experimental values, see Ref. [5] and references therein. The G2MP2 values of the reaction enthalpy are in excellent agreement with

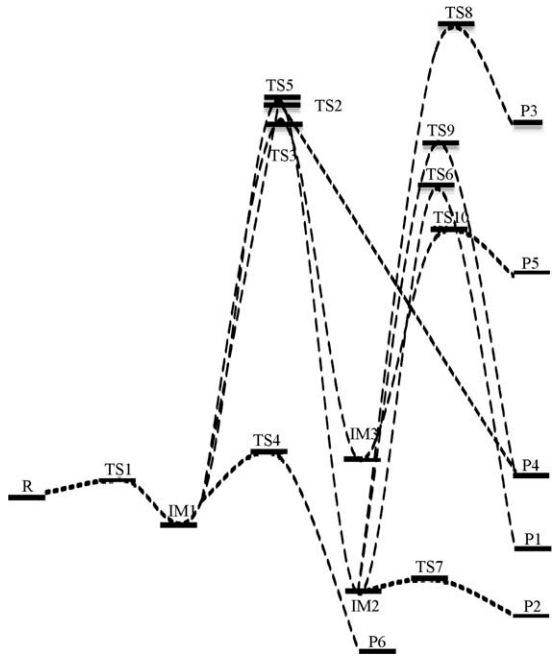

FIGURE 2. Schematic energy profile of the PES for the CH_3Cl + OH reaction system at the G2MP2 level.

the experimental results, so the most reliable results are obtained at this level. The moments of inertia and vibrational frequencies for various species for the CH_3Cl + OH reaction at the MP2/6-311+G (d, p) level of theory are listed in Table II.

3.1. MECHANISMS

The reaction of CH_3Cl with OH starts with the formation of intermediate IM1 via the transition state TS1. All the vibrational frequencies of IM1 are positive, which indicates the molecular complex IM1 is a stable structure. The molecular complex IM1 is 1.0 kcal/mol below the reactants at the G2MP2 method. The C–Cl bond in IM1 is broken to generate IM2 surmounting the barrier of TS2. The broken C–Cl bond is elongated to be 2.27 Å and the new formed C–O bond is 1.93 Å, the barrier of TS2 is 49.5 kcal/mol. With so high a barrier height this reaction does not occur at low temperature. From IM2, four rearrangement scenarios are possible to form different products. (1) CH_3O + HCl formation: The IM2 can dissociate to product P1 (CH_3O + HCl) with the O–H bond scission. The corresponding TS is TS6, in which the broken O–H bond is 1.49 Å, and the formed H-Cl bond is shortened to 1.97 Å and it gets near to the C–Cl bond in HCl (product). The energy of TS6 is 38.4 kcal/mol higher than that of the reactants. (2) CH_2OH + HCl formation: The H atom in OH (CH_3OH) is abstracted by Cl radical to produce P2 (CH_2OH + HCl) via the transition state TS7. In TS7, the H–Cl bond is shortened by 0.75 Å and the C–H bond is lengthened by 0.08 Å, the barrier of TS7 is 11.0 kcal/mol below the reactants. (3) CH_3OCl + H formation: With the Cl atom approaching to the O atom in CH_3OH, the product P3 (CH_3OCl + H) is generated via the transition state TS8 and the barrier of TS8 is 55.9 kcal/mol. In this process, with the stretching of the O–H bond, the atom Cl shifts to O atom and forms a new O–Cl bond. (4) $ClCH_2OH$ + H formation: One of the H atoms in CH_3 is abstracted

TABLE I

Relative energies and ZPE corrections of reactants, IMs, TSs, and products involved in the CH_3Cl + OH reaction, in kcal/mol (bold type shows the reaction enthalpy).

Species	ZPE	G2	G2MP2	Other works
R(CH_3Cl + OH)	29.65	0.00	0.00	
IM1	31.94	−1.06	−1.06	
IM2	33.45	−12.99	−12.67	
IM3	30.81	4.29	4.26	
TS1	31.15	1.63	1.60	
TS2	31.87	49.06	49.55	
TS3	31.32	47.43	47.01	
TS4	27.77	5.39	3.89	
TS5	28.60	50.03	49.80	
TS6	28.83	38.25	38.38	
TS7	30.60	−11.15	−11.02	
TS8	28.18	56.01	55.89	
TS9	29.02	44.55	44.08	
TS10	29.04	32.00	32.31	
P1(CH_3O+HCl)	28.10	−6.26	−6.11	
		−8.76	**−6.12**	
P2(CH_2OH+HCl)	28.38	−15.05	−15.47	
		−17.55	**−15.28**	
P3(CH_3OCl+H)	26.71	46.86	46.40	
		43.78	**46.35**	
P4($ClCH_2OH$+H)	27.81	3.87	3.31	
		3.73	**3.17**	
P5(CH_3+ClOH)	27.18	27.65	27.45	**27.21**[b]
		28.18	**27.98**	
P6(CH_2Cl+H_2O)	28.25	−19.10	−19.65	**−19.48**[a]
		−18.86	**−19.41**	**−19.43**[a]
				−16.61[a]
				−20.62[b]

[a] Ref. [5].
[b] Ref. [9].

TABLE II

Vibrational frequencies (cm^{-1}) and moments of inertia (amu) for various species for the CH_3Cl + OH reaction at the MP2/6-311+G (d, p) level of theory.

Species	I_a, I_b, I_c	Frequencies
CH_3	6.3,6.3,12.6	461,1446,1446,3166,3359,3359
		501,1450,1450,3201,3372,3372[b]
OH	3.2	3838
		3837[b]
H_2O	2.2,4.1,6.3	1628,3886,4005
		1650,3872,3993[b]
HCl	5.6,5.6	3087
HOCl	2.9,121.9,124.9	731,1211,3833
		774,1276,3819[b]
CH_3OCl	43.1,290.9,322.6	267,370,677,1055,1192,1211,1483,1486,1524,3068,3157,3193
$ClCH_2OH$	45.8,318.8,348.6	358,447,741,993,1125,1222,1393,1427,1517,3124,3224,3878
CH_2OH	9.4,60.3,68.8	445,696,1079,1218,1380,1518,3182,3335,3908
CH_3O	11.4,65.3,65.6	806,983,1132,1424,1431,1545,3016,3099,3135
CH_2Cl	6.4,110.5,116.9	140,943,1056,1492,3233,3377
		272,843,1028,1460,3240,3347[a]
		156,881,1026,1465,3266,3401[b]
CH_3Cl	11.4,134.5,134.5	792,1069,1069,1445,1495,1495,3109,3215,3215
		751,1048,1048,1411,1513,1513,3132,3240,3240[a]
		777,1048,1048,1405,1516,1516,3134, 3228,3228[b]
IM1	89.9,365.3,443.2	105,109,307,484,582,760,1056,1070,1446,1513,1521,3106,3202,3269,3817
IM2	51.9,524.6,559.8	80,108,195,428,1063,1085,1194,1369,1502,1518,1528,3071,3151,3207,3893
IM3	45.2,478.9,508.1	45,90,155,283,513,606,1012,1016,1382,1480,1484,3127,3152,3254,3849
TS1	114.6,362.3,465.6	371i,150,174,319,480,762,1021,1047,1418,1446,1501,3127,3217,3300,3823
TS2	125.5,261.6,370.4	1075i,109,276,453,609,782,978,1058,1370,1457,1519,3176,3320,3344,3823
TS3	109.4,284.9,376.7	329i,47,347,503,711,820,859,895,1257,1448,1455,3146,3321,3330,3768
TS4	81.8,483.2,552.9	1944i,60,115,265,732,790,856,1044,1134,1274,1451,1470,3154,3252,3829
		2182i,44,117,261,707,757,853,1026,1150,1260,1454,1481,3167,3267,3814[a]
		1935i,113,114,318,718,799,877,1036,1150,1304,1452,1491,3165,3255,3814[b]
TS5	72.4,322.3,375.4	1671i,258,320,576,733,770,956,1010,1050,1326,1424,1618,2978,3163,3824
TS6	58.5,550.7,585.6	3243i,86,143,188,1054,1092,1144,1195,1428,1481,1493,1529,3051,3136,3146
TS7	57.1,625.8,666.6	320i,86,204,438,1011,1092,1143,1277,1334,1405,1502,1709,3100,3213,3888
TS8	56.9,300.6,344.2	2277i,185,254,347,572,892,1081,1181,1198,1467,1495,1516,3098,3200,3225
TS9	54.9,411.9,439.7	2191i,121,297,482,674,819,999,1130,1266,1315,1404,1547,3154,3228,3861
TS10	26.1,532.5,542.6	871i,96,169,185,209,506,561,954,1098,1443,1449,3162,3346,3355,3858

[a] Ref. [5].
[b] Ref. [9].

by Cl radical to produce P4 ($ClCH_2OH$ + H) via the transition state TS9. The energy TS9 is 56.8 kcal/mol higher than that of the intermediate IM2, and the intermediate IM2 is 11.7 kcal/mol more stable than IM1.

Additionally, IM1 via the transition state TS3 can generate IM3. The formation of the addition complex IM3 is due to the electrostatic effect of the CH_3Cl close up to the OH. Then a Cl atom migrates via TS10 to yield product P5 (CH_3 + HOCl). In the Cl-abstraction reaction the O–Cl bond is shortened by 0.44 Å, and it arrives to the O–Cl bond in HOCl (product) and the C–Cl bond is lengthened by 0.56 Å.

Furthermore, from IM1, two other scenarios are possible to form different products. The first one is formation of P6 (CH_2Cl + H_2O), the reaction pathway is abstraction of a hydrogen atom in the CH_3 group of IM1 to produce P6 via TS4. In the H-abstraction reaction, as shown in Figure 1, the formed O–H bond is shortened to 1.31 Å and it draws near to the O–H bond in H_2O (product) and the broken C–H bond is 1.18 Å. The barrier at TS4 is 6.4 kcal/mol higher than that at the

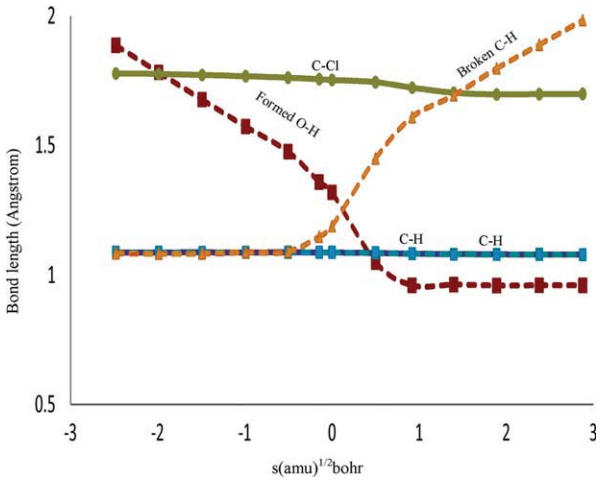

FIGURE 3. The changing of some key bond distances along the reaction coordinate for P4 channel at the MP2/6-311+G (d, p) level. [Color figure can be viewed in the online issue, which is available at wileyonlinelibrary.com.]

intermediate IM1. The second pathway from IM1 is forming product P4 via the transition state TS5. In TS5, whose energy is 49.8 kcal/mol higher than the reactants, the broken C–H bond and formed C–O bond are 1.27 and 1.67 Å, respectively.

Regarding the mechanisms stated above, the dominant channel of the title reaction is abstraction of a hydrogen atom in the CH_3 group of IM1 followed by dissociation to the final product P6 ($CH_2Cl + H_2O$). Although other channels cannot take place at room temperature, because they have high barriers, we calculated the rate constants for all of the channels for formation of different products to study dependence of the rate constants and branching ratio on the temperature.

Because the dominant channel is P6 channel, the changes of the bond length along the minimum energy path (MEP) for this channel via TS4 as a function of the IRC, s, are described in Figure 3. It appears that for this reaction, the active O–H and C–H bonds change strongly in the course of the reaction, and the other bond lengths are almost invariant during the reaction process. The breaking C–H bond elongates linearly with s after about $s = -0.5$ (amu)$^{1/2}$bohr, and the forming O–H bond shortens rapidly and arrives at the bond length of O–H in H_2O molecule at about $s = 1.0$ (amu)$^{1/2}$bohr. Thus, it is evident that the geometric changes mainly take place in the region of s from -0.5 to 1.0 (amu)$^{1/2}$bohr. Similar conclusions can also be obtained for other channels.

Additionally, the classical potential energy (V_{MEP}), the ground-state vibrational adiabatic potential energy (V_a^G) and the ZPE as functions of the IRCs for this channel at the G2MP2 level are plotted in Figure 4, where $V_a^G(s) = V_{MEP}(s) + ZPE(s)$. The position of the maximum of V_{MEP} is almost the same as that of V_a^G, and the ZPE curve is constant in the vicinity of the saddle point as can be seen from this figure.

3.2. RATE CONSTANT CALCULATION

The reaction scheme used in the calculation is as follows:

$$\mathrm{CH_3Cl + OH} \quad (\mathrm{R}) \underset{1}{\overset{0}{\rightleftarrows}} \mathrm{IM1^*} \underset{3}{\overset{2}{\rightleftarrows}} \mathrm{IM2^*}$$

$$\mathrm{IM2^*} \xrightarrow{8} \mathrm{CH_3O + HCl} \quad (\mathrm{P1})$$

$$\mathrm{IM2^*} \xrightarrow{9} \mathrm{CH_2OH + HCl} \quad (\mathrm{P2})$$

$$\mathrm{IM2^*} \xrightarrow{10} \mathrm{CH_3OCl + H} \quad (\mathrm{P3})$$

$$\mathrm{IM2^*} \xrightarrow{11} \mathrm{ClCH_2OH + H} \quad (\mathrm{P4})$$

$$\mathrm{IM1^*} \underset{5}{\overset{4}{\rightleftarrows}} \mathrm{IM3^*} \xrightarrow{12} \mathrm{CH_3 + ClOH} \quad (\mathrm{P5})$$

$$\mathrm{IM1^*} \xrightarrow{6} \mathrm{CH_2Cl + H_2O} \quad (\mathrm{P6})$$

$$\mathrm{IM1^*} \xrightarrow{7} \mathrm{ClCH_2OH + H} \quad (\mathrm{P4})$$

$$\mathrm{IMj^*} \xrightarrow{\omega_i} \mathrm{IMj}$$

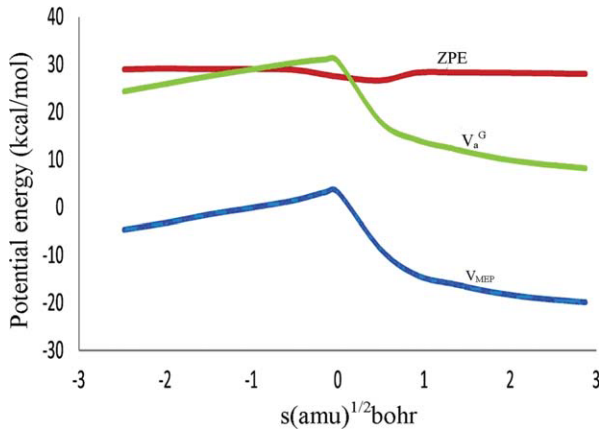

FIGURE 4. Classical potential energy (V_{MEP}), vibrational adiabatic potential energy (V_a^G) and ZPE as a function of the IRC, s, at G2MP2 method for P4 channel. [Color figure can be viewed in the online issue, which is available at wileyonlinelibrary.com.]

Steady-state assumption for all the excited IMs leads to the following expressions for the second-order rate constants of various product channels:

$$k_{CH_3O+HCl}\ (T,P) = \frac{l_a}{h}\frac{Q_t^{\neq}Q_r^{\neq}}{Q_{CH_3Cl}\ Q_{OH}}e^{-E_a/RT} \int_0^{\infty}\frac{k_2k_8X_3}{Y}N_0(E^{\neq})e^{-E^{\neq}/RT}dE^{\neq}$$

$$k_{CH_2OH+HCl}\ (T,P) = \frac{l_a}{h}\frac{Q_t^{\neq}Q_r^{\neq}}{Q_{CH_3Cl}\ Q_{OH}}e^{-E_a/RT} \int_0^{\infty}\frac{k_2k_9X_3}{Y}N_0(E^{\neq})e^{-E^{\neq}/RT}dE^{\neq}$$

$$k_{CH_3OCl+H}\ (T,P) = \frac{l_a}{h}\frac{Q_t^{\neq}Q_r^{\neq}}{Q_{CH_3Cl}\ Q_{OH}}e^{-E_a/RT} \int_0^{\infty}\frac{k_2k_{10}X_3}{Y}N_0(E^{\neq})e^{-E^{\neq}/RT}dE^{\neq}$$

$$k_{ClCH_2OH+H}\ (T,P) = \frac{l_a}{h}\frac{Q_t^{\neq}Q_r^{\neq}}{Q_{CH_3Cl}\ Q_{OH}}e^{-E_a/RT} \int_0^{\infty}\frac{k_2k_{11}X_3 + k_7k_2X_3}{Y}N_0(E^{\neq})e^{-E^{\neq}/RT}dE^{\neq}$$

$$k_{CH_3+ClOH}\ (T,P) = \frac{l_a}{h}\frac{Q_t^{\neq}Q_r^{\neq}}{Q_{CH_3Cl}\ Q_{OH}}e^{-E_a/RT} \int_0^{\infty}\frac{k_4k_{12}X_2}{Y}N_0(E^{\neq})e^{-E^{\neq}/RT}dE^{\neq}$$

$$k_{CH_2Cl+H_2O}\ (T,P) = \frac{l_a}{h}\frac{Q_t^{\neq}Q_r^{\neq}}{Q_{CH_3Cl}\ Q_{OH}}e^{-E_a/RT} \int_0^{\infty}\frac{k_6k_2X_3}{Y}N_0(E^{\neq})e^{-E^{\neq}/RT}dE^{\neq}$$

$$k_{IM1}\ (T,P) = \frac{l_a}{h}\frac{Q_t^{\neq}Q_r^{\neq}}{Q_{CH_3Cl}\ Q_{OH}}e^{-E_a/RT} \int_0^{\infty}\frac{\omega X_2X_3}{Y}N_0(E^{\neq})e^{-E^{\neq}/RT}dE^{\neq}$$

$$k_{IM2}\ (T,P) = \frac{l_a}{h}\frac{Q_t^{\neq}Q_r^{\neq}}{Q_{CH_3Cl}\ Q_{OH}}e^{-E_a/RT} \int_0^{\infty}\frac{\omega k_2X_3}{Y}N_0(E^{\neq})e^{-E^{\neq}/RT}dE^{\neq}$$

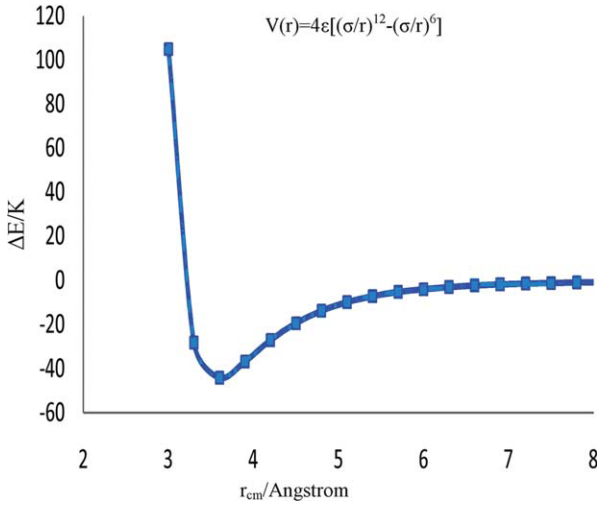

FIGURE 5. The MP2/6-311+G (d, p) calculated intermolecular interaction energy between the IM1 and the helium bath gas. r_{cm} represents the separation of the center of mass of the IM1 and He. [Color figure can be viewed in the online issue, which is available at wileyonlinelibrary.com.]

$$k_{IM3}\ (T,P) = \frac{l_a}{h}\frac{Q_t^{\neq}Q_r^{\neq}}{Q_{CH_3Cl}\ Q_{OH}}e^{-E_a/RT} \int_0^{\infty}\frac{\omega k_4X_2}{Y}N_0(E^{\neq})e^{-E^{\neq}/RT}dE^{\neq}$$

with the following definitions:

$$X_1 = k_1 + k_2 + k_4 + k_6 + k_7 + \omega$$
$$X_2 = k_3 + k_8 + k_9 + k_{10} + k_{11} + \omega$$
$$X_3 = k_5 + k_{12} + \omega$$
$$Y = \frac{X_2X_3}{X_1X_2X_3 - k_2k_3X_3 - k_4k_5X_2}$$

where l_a is the statistical factor (degeneracy) for the association step. $Q_t^{\neq}$ and $Q_r^{\neq}$ are the translational and rotational partition functions of the variational "transition state" for the association, respectively. $Q_{CH_3\ Cl}$ and Q_{OH} are the total partition functions of CH_3Cl and OH, respectively. E_a is the barrier for the association. $N_0(E^{\neq})$ is the number of state for the association "transition state." The overall rate constant corresponds to the sum of the above nine rate constants. The branching ratios for each product channel are calculated as the ratio of the individual rate constants to the overall rate constant.

TABLE III

Calculated rate constants ($cm^3 molecule^{-1} s^{-1}$) for the CH_3Cl + OH reaction in the temperature range 200–2000 K.

k_{exp}[b]	k[a]	k_t	k_{P6}	k_{P5}	k_{P4}	k_{P3}	k_{P2}	k_{P1}	k_{IM3}	k_{IM2}	k_{IM1}	T (K)
4.63E−15	5.12E−15	4.73E−15	4.20E−15	9.34E−19	1.36E−18	7.55E−22	1.55E−18	1.68E−19	3.92E−18	6.08E−19	5.28E−16	**200**
1.62E−14	1.77E−14	1.69E−14	1.46E−14	2.23E−18	3.83E−18	1.79E−21	4.65E−18	3.65E−19	1.41E−17	2.22E−18	2.29E−15	**250**
2.47E−14	2.70E−14	2.61E−14	2.24E−14	3.17E−18	5.24E−18	2.37E−21	6.71E−18	4.91E−19	2.21E−17	3.48E−18	3.64E−15	**273**
3.63E−14	3.98E−14	3.79E−14	3.24E−14	4.03E−18	7.03E−18	2.90E−21	8.91E−18	5.44E-19	3.09E−17	4.74E−18	5.43E−15	**298**
3.72E−14	4.09E−14	3.82E−14	3.26E−14	4.23E−18	7.04E−18	2.89E−21	8.94E−18	5.41E−19	3.29E−17	4.81E−18	5.53E−15	**300**
[c]n/a	7.64E−14	7.04E−14	5.93E−14	7.42E−18	1.18E−17	4.60E−21	1.62E−17	8.35E−19	6.18E−17	9.36E−18	1.10E−14	**350**
[c]n/a	1.26E−13	1.18E−13	9.97E−14	1.13E−17	1.73E−17	5.44E−21	2.09E−17	8.60E−19	1.01E−16	1.21E−17	1.76E−14	**400**
[c]n/a	2.72E−13	2.34E−13	2.01E−13	2.53E−17	3.43E−17	1.27E−20	5.07E−17	1.71E−18	2.14E−16	2.84E−17	3.31E−14	**500**
[c]n/a	5.00E−13	4.56E−13	3.98E−13	5.88E−17	7.10E−17	2.87E−20	1.10E−16	3.16E−18	4.21E−16	5.61E−17	5.74E−14	**600**
[c]n/a	1.29E−12	1.05E−12	9.58E−13	2.14E−16	2.51E−16	1.05E−19	2.23E−16	1.06E−17	1.04E−15	1.26E−16	9.22E−14	**800**
[c]n/a	2.68E−12	1.75E−12	1.65E−12	6.07E−16	4.03E−16	2.80E−19	6.86E−16	1.72E−17	1.79E−15	1.77E−16	1.03E−13	**1000**
[c]n/a	4.89E−12	3.37E−12	3.23E−12	1.88E−15	1.13E−15	8.55E−19	1.61E−15	4.34E−17	3.36E−15	2.81E−16	1.34E−13	**1200**
[c]n/a	1.01E−11	8.64E−12	8.43E−12	8.42E−15	4.19E−15	4.27E−18	5.11E−15	1.71E−16	7.39E−15	5.16E−16	1.82E−13	**1500**
[c]n/a	1.82E−11	1.58E−11	1.56E−11	2.39E−14	1.13E−14	1.52E−17	1.17E−14	4.98E−16	1.08E−14	6.96E−16	1.93E−13	**1800**
[c]n/a	2.54E−11	1.74E−11	1.71E−11	3.13E−14	1.62E−14	2.31E−17	1.45E−14	7.13E−16	1.22E−14	8.18E−16	1.98E−13	**2000**

[a] Ref. [9].
[b] Ref. [30].
[c] n/a: not available.

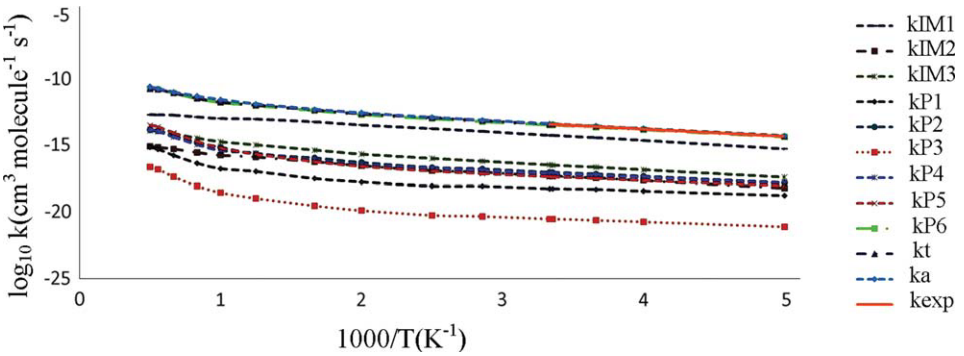

FIGURE 6. The logarithm of calculated rate constants as a function of $10^3/T$ for the $CH_3Cl + OH$ reaction. [a]Ref. [9] and [b]Ref. [30]. [Color figure can be viewed in the online issue, which is available at wileyonlinelibrary.com.]

The microcannonical rate constants are calculated using RRKM theory as follows:

$$k_i(E) = \alpha_i \kappa_i C_i \frac{N(E - E_i^*)}{h p_j(E)},\ i = 1, 2, \ldots, 12; j = 1, 2, 3$$

where α_i is the statistical factor for reaction path degeneracy [20], κ_i is the tunneling factor that was considered using the Eckart potential [21], C_i is the ratio of the overall rotational partition function of the TSi (i = 1, 2,…, 10) and the intermediate IMj (1, 2, 3), h is the Planck's constant, $\rho_j(E)$ is the density of states at energy E of the intermediate j, and $N(E - E_i^*)$ is the number of states at the energy above the barrier height E_i^* for TS i. Because several structures have small vibrational frequencies below 100 cm^{-1}, as shown in Table II, a rotor approximation [22–25] was used in the multichannel RRKM calculations. The density of states and the number of states are calculated using the Beyer-Swinehart algorithm [26, 27]. The collision deactivation rate $\omega = \beta_c Z_{LJ}[He]$, where β_c is the collision efficiency calculated using Troe's weak collision approximation [28] with the energy transfer parameter $-\langle \Delta E \rangle$. Z_{LJ} is the Lennard-Jones collision frequency. [He] is the concentration of the helium bath gas. The tunneling effect was considered using the Eckart potential. The weak collision approximation is used for each IM, and the collisional rates are assumed to be the same for all IMs for simplicity [29]. The collision efficiency is estimated using the Lennard–Jones potential by fitting the interaction energies calculated at the MP2/6-311+G (d, p) level for IM1...He, and the potential well (ε = 44.09 K) and the collisional diameter (σ = 3.6 Å) are estimated (Fig. 5).

The RRKM-calculated total and individual rate constants over the temperature range of 200–2000 K and at a pressure of 760 Torr are collected in Table III and compared with the experimentally known values [30] and obtained results by Tzima et Al. [9]. At the temperatures 273–300 K, the total rate constants are in excellent agreement with available experimental values. Figure 6 shows the plots of rates versus temperature. As Figure 6 shows the total rate constants that vary with temperature. Over the temperature range of 200–2000 K, the total rate constants are fitted to a three-parameter expression, which can be described as follows with the units of $cm^3 molecule^{-1} s^{-1}$.

$$k = 2.86 \times 10^{-11} T^{-00.2} e^{\frac{-2779.7}{T}}$$

The energy transfer parameter, $-\langle \Delta E \rangle$, i.e., the average energy transferred per collision, is unknown and cannot be calculated quantitatively.

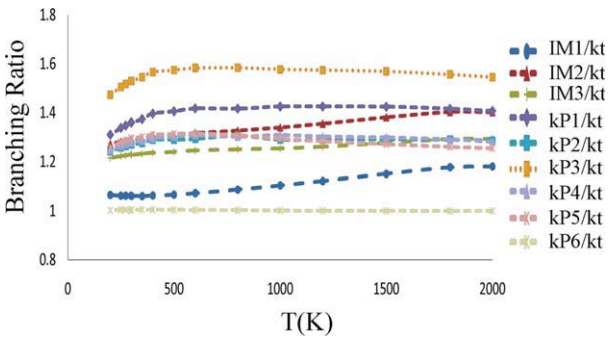

FIGURE 7. The calculated branching ratio for the reaction $CH_3Cl + OH$ as a function of T (K). [Color figure can be viewed in the online issue, which is available at wileyonlinelibrary.com.]

In consideration of the experimental rate constants measured at different pressures, it is estimated by Lim and Gilbert's biased random walk (BRW) model (200–1000 K) $-\langle\Delta E\rangle/\mathrm{cm}^{-1} = 0.6\mathrm{T}–41$ for Helium [31]. As seen in Figure 6, the main channel is P6 and the other channels such as IM, IM2, IM3, P1, P2, P3, P4, and P5 are negligible. The branching ratios are depicted for each channel in Figure 7. All the results agree about the weak temperature dependences of these branching ratios.

4. Conclusions

In this article, the mechanism and kinetics of CH_3Cl with OH were investigated using *ab initio* methods along with RRKM theory. The results show that the dominant channel is the addition of reactants to form IM1 and then decomposes to $CH_2Cl + H_2O$. The results are in good agreement with the available experimental value at temperature 200–300 K. Over the temperature range of 200–2000 K, the overall rate constants can be described as follows in unit of cm^3 $molecule^{-1}$ s^{-1}.

$$k = 2.86 \times 10^{-11} T^{-00.2} e^{\frac{-2779.7}{T}}$$

References

1. Hsu, K. J.; DeMore, W. B. Geophys Res Lett 1994, 21, 805.
2. Herndon, S. C.; Gierczak, R. K.; Talukdar, K.; Ravishankara, A. R. Phys Chem Chem Phys 2001, 3, 4529.
3. Rhew, R. C.; Miller, B. R.; Weiss, R. F. Nature 2000, 403, 292.
4. Yokouchi, Y.; Noijiri, Y.; Barrie, L. A.; Toom-Sauntry, D.; Machida, T.; Inuzuka, Y.; Akimoto, H.; Li, H. J.; Fujinuma, Y.; Aoki, S. Nature 2000, 403, 295.
5. Louis, F.; Gonzalez, C. A.; Huie, R. E.; Kurylo, M. J. J Phys Chem A 2000, 104, 8773.
6. Sheng, L.; Li, Z.-S.; Liu, J.-Y.; Xiao, J.-F.; Sun, C.-C. J Chem Phys 2003, 118, 4920.
7. EI-Taher, S. Int J Quant Chem 2001, 84, 426.
8. Bottni, A.; Poggi, G.; Emmi, S. S. J Mol Struct 1993, 279, 299.
9. Tzima, T. D.; Papayannis, D. K.; Melissas, V. S. J Chem Phys 2005, 312, 169.
10. Frisch, M. J.; Trucks, G. W.; Schlegel, H. B.; Scuseria, G. E.; Robb, M. A.; Cheeseman, J. R.; Zakrzewski, J. A.; Montgomery, J. A. Jr.; Stratmann, R. E.; Burant, J. C.; Dapprich, S.; Millam, J. M.; Daniels, A. D.; Kudin, K. N.; Strain, M. C.; Farkas, O.; Tomasi, J.; Barone, V.; Cossi, M.; Cammi, B.; Mennucci, B.; Pomelli, C.; Adamo, C.; Clifford, S.; Ochterski, J. W.; Petersson, G. A.; Ayala, P. Y.; Cui, Q.; Morokuma, K.; Rega, N.; Salvador, P.; Dannenberg, J. J.; Malick, D. K.; Rabuck, A. D.; Raghavachari, K.; Foresman, J. B.; Cioslowski, J.; Ortiz, J. V.; Baboul, A. G.; Stefanov, B. B.; Liu, G.; Liashenko, A.; Piskorz, P.; Komaromi, I.; Gomperts, R.; Martin, R. L.; Fox, D. J.; Keith, T.; Al-Laham, M. A.; Peng, C. Y.; Nanayakkara, A.; Challacombe, M.; Gill, P. M. W.; Johnson, B.; Chen, W.; Wong, M. W.; Andres, J. L.; Gonzalez, C.; Head-Gordon, M.; Replogle, E. S.; Pople, J. A. Gaussian 03 (Revision B.03); Gaussian, Inc.: Pittsburgh, PA, 2003.
11. Gonzales, C.; Schlegel, H. B. J Chem Phys 1989, 90, 2154.
12. Gonzales, C.; Schlegel, H. B. J Phys Chem 1990, 94, 5523.
13. Fukui, K. Acc Chem Rev 1981, 14, 363.
14. Curtiss, L. A.; Raghavachari, K. J.; Pople, A. J Chem Phys 1993, 98, 1293.
15. Chase, M. W. Jr. NIST-JANAF Thermochemical Tables, 4th ed.; J Phys Chem Ref Data 1998, Monograph 9.
16. Chase, M. W. Jr.; Davies, C. A.; Downey, J. R. Jr.; Frurip, D. J.; McDonald, R. A.; Syverud, A. N. JANAF Thermochemical Tables, 3rd ed.; National Bureau of Standards: Washington, DC, 1985; Vol. 14.
17. Kuchitsu, K. Structure of Free Polyatomic Molecules Basic Data - Data in Science & Technology; Springer-Verlag: Berlin and Heidelberg GmbH & Co. K, 1998; Vol. 1, p 94, 104.
18. Benedict, W. S.; Gailor, N.; Plyler, E. K. J Chem Phys 1956, 24, 1139.
19. Escribano, R. M.; Di Lonardo, G.; Fusina, L. Chem Phys Lett 1996, 259, 614.
20. Holbrook, K. A.; Pilling, M. J.; Robertson, S. H. Unimolecular Reactions; John Wiley: Chichester, UK, 1996.
21. Johnston, H. S.; Heicklen, J. J Phys Chem 1962, 66, 532.
22. Ayala, P. Y.; Schlegel, H. B. J Chem Phys 1998, 108, 2314.
23. Truhlar, D. G. J. Comput Chem 1991, 12, 266.
24. Pitzer, K. S. Quantum Chemistry; Prentice-Hall: Englewood Cliffs, NJ, 1953.
25. Pitzer, K. S.; Gwinn, W. D. J. Chem. Phys. 1942, 10, 428–440.
26. Stein, S. E.; Rabinovitch, B. S. J Chem Phys 1973, 58, 2438.
27. Astholz, D. C.; Troe, J.; Wieters, W. J Chem Phys 1979, 70, 5107.
28. Troe, J. J Chem Phys 1977, 66, 4745.
29. Marchand, N.; Rayez, J. C.; Smith, S. C. J Phys Chem A 1998, 102, 3358.
30. Sander, S. P.; Finlayson-Pitts, B. J.; Friedl, R. R.; Golden, D. M.; Huie, R. E.; Kolb, C. E.; Kurylo, M. J.; Molina, M. J.; Moortgat, G. K.; Orkin, V. L.; Ravishankara, A. R. Chemical Kinetics and Photochemical Data for Use in Atmospheric Studies, Evaluation Number 14, JPL Publication 02–25, Jet Propulsion Laboratory, Pasadena, 2002.
31. Lim, K. F.; Gilbert, R. G. J Chem Phys 1990, 92, 1819.